

Large Scale Forming of Non-Crimp Fabrics for Aerostructures

Claudia Jimenez Martin^{1,2,a*}, Vincent Maes^{2,b}, Turlough McMahon^{1,c}
and James Kratz^{2,d}

¹Airbus UK, Pegasus House, Aerospace Ave, Filton, Bristol BS34 7PA, UK

²The Bristol Composites Institute, Queen's Building, University Walk, Bristol BS8 1TR, UK

^aclaudia.jimenezmartin@bristol.ac.uk, ^bvincent.maes@bristol.ac.uk, ^cJames.Kratz@bristol.ac.uk,

^dturlough.mcmahon@airbus.com

Keywords: Non-Crimp Fabrics, forming, dry fibre process

Abstract. The increased production rate targets of the aerospace industry have driven the development of dry fibre infusion processes. Biaxial Non-Crimp Fabrics (NCFs) are considered in this work due to their potential high deposition rates and higher mechanical performance to woven fabrics. Forming is an integral step prior to infusion and curing. Understanding the forming behaviour of NCFs at scale is therefore key to achieving high quality parts. To investigate the draping and shearing behaviour of NCFs, geometries with complexities associated with the composite structure are used. This study presents an experimental campaign on two large scale (2 metres in span) geometries with complexities representative of aerostructures. The combination of features such as ramps and curvature with corner radii leads to distinctive out-of-plane wrinkling. The relationship between geometry, material and resulting preform quality is observed through the use of 3D scans. Results show differing preform quality in terms of wrinkling phenomena, showing the importance of geometry of choice for material drapability tests at an industrial scale.

1. Introduction

The commercial aerospace industry is shifting to high-rate processes for the next generation aircraft. Out-of-autoclave dry fibre technology is one of the processes that has the potential to meet the increase in production rate targets. A key step prior to curing is the forming of the reinforcement material into the final part geometry [1]. In-plane shear is the dominant deformation mechanism in forming [2], resulting in large rotations in the fibre direction and a change in the net shape of the material [3]. Non-Crimp Fabrics (NCFs) are chosen for their higher mechanical properties by comparison to conventional woven fabrics [2], due to their fibres being stitched instead of woven. However, this architecture affects the shear behaviour, as the 'cross-over points' between tows around which rotation occurs are not present in stitched NCFs. This can lead to other mechanisms of deformation such as undesirable out-of-plane wrinkling causing a knockdown on the mechanical performance of the final component.

To investigate the forming and shearing behaviour of NCFs, geometries with complexities associated with the composite structure are used. To minimise cost intensive testing at full scale, a building block approach is employed. Figure 1 shows the building block approach for mechanical testing, with levels 2, 3 and 4 showing the scale and type of geometries commonly used for an assessment on drapability. Drapability and formability are used interchangeably in this study as the tests often involve the 'draping' of a fabric over a mould.

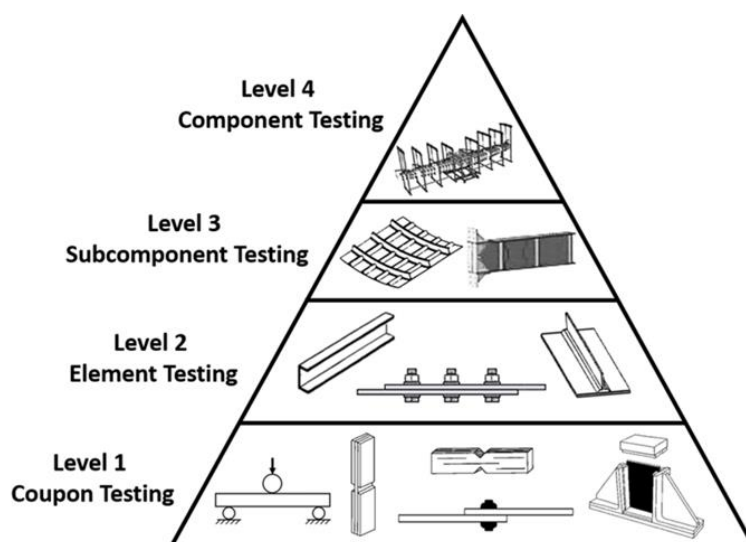


Figure 1. Adapted from [4]. Building block approach for mechanical testing of composite aerostructures

This study presents an experimental campaign on two subcomponent sized geometries with complexities seen in aerostructures. The main research gaps this study addresses is the effect of geometry and NCF fabric fibre orientation, two key parameters driving forming defects, on a large scale preform. The geometries chosen and their larger size compared to most geometries used in the literature lead to an analysis that is industrially relevant. The biaxial NCFs tested are representative orientations of layups for structures, with combinations of 0° , 45° and 90° fibres. The study uses single diaphragm forming over a male tool. Overall, the study aims to address two challenges of the industrial testing pyramid for dry fibre preforming:

- The choice of geometrical complexities that are tested at the subcomponent scale
- The contribution of each biaxial NCF format to the overall preform quality.

2. Literature Review

2.1. Complex geometries – a discussion

The interaction between part geometry and fabric mechanical properties is well known in the industry of composite fabrics [5][6]. As a result, the term ‘complex geometry’ has been coined and used extensively in the realm of dry fabric forming studies. It encompasses anything from three dimensional shapes such as hemispheres and tetrahedrons [7] to those assimilating real life structures such as Hallander’s spar geometry [8]. Studies relating to the automotive industry deploy geometries that may even resemble the full structure, as seen in Nezami et al.’s publication [6]. The advantage of this is the amount of fabric (e.g. ply size) draped, and therefore size of defects indicative of preform quality, is similar in size to that of the actual component. By comparison, Hallander’s spar geometry is an order of magnitude smaller than those of interest for this study [9]. Two limitations arise from this disparity in size between ‘test geometry’ and full scale component geometry: the size of defects such as out-of-plane wrinkling is smaller than those likely to be observed at full scale; and the proportion of the ‘free’ fibre length at the edge of the ply to the ‘constrained’ fibre length in the centre is much higher, i.e. the edge effects increase as the preform size decreases. Though the automotive industry may be able to benefit from full scale geometries for drapability assessments, primary aerostructures being much larger in size may still require the building block approach shown in Figure 1.

Table 1 provides a summary of the most common test geometries employed in drapability studies. Tests widely available in the literature of the likes of the hemisphere or punch tests have their own limitations. Perhaps the most noticeable is that the preform is loaded in tension during a punch test, whereas in a forming process, the preform may experience compression and in-plane shear as well as tension. The industry seems to be moving towards these testing methods for drapability with the new release of the Drapetest ISO standard [10]. Though moving towards a standardised drapability test may sound progressive, it is naïve to think this could replace draping trials over representative

geometries. Regardless of the limitations tests like the hemisphere punch present, their use continues to be widespread as it is a convenient size and shape test bed. Its use has led to extensive studies from the effect of blank holder force [11] to the application of new machine vision inspection techniques [11], even being used in studies alongside representative automotive geometries [6] to de-risk the forming process. Nevertheless, to obtain an idea for scale and type of defects expected due to geometrical complexities in full scale industrial components - especially structures that are orders of magnitude bigger than those listed in Table 1 - a larger size geometry offers clear advantages.

Table 1. Summary of geometries used in the literature for drapability studies including size, process used, material and application

Geometry	Size 1 (mm)	Size 2 (mm)	Size 3 (mm)	Process	Material	Application	Ref
Boomerang	330	164	-	Matched tool forming + blank holder	Plain woven carbon	All sectors	[12]
C spar	480	70	55	Vacuum (single diaphragm) hot drape forming (HDF)	UD prepreg	Aerostructures	[8] [13] [14]
Complex automotive	-	-	-	Matched tool forming + blank holder	Plain woven carbon w/ binder	Automotive	[6]
Double dome	500	300	-	Press thermoforming	Cross-ply thermoplastic prepreg	-	[15]
Double dome	470	270	-	Matched tool forming + blank holder	Plain woven glass	Aeronautic	[16]
Doubly symmetric exaggerated	230	50	25	Matched tool forming	Twill woven glass	-	[17]
Hemisphere	200	200	100	Punch / open die + blank holder	Plain woven carbon	All sectors	[12]
Hemisphere	150	150	75	Punch / open die + blank holder	Biaxial / triaxial NCF	Transport / automotive	[18]
Hemisphere	150	150	75	Punch / open die + blank holder	Plain woven glass	-	[19]
Hemisphere	100	100	50	Punch / open die + blank holder	Biaxial NCF	-	[11]
Prismatic shape	280	280	175	Punch / open die + blank holder	Dry woven (carbon)	Automotive / aeronautic	[5]
Tetrahedron	265	128	-	Punch / open die + blank holder	Flax woven	Automotive	[7]

2.2.NCFs' formability issue

A review of the literature reveals the additional challenges with forming of NCFs by comparison to their woven counterparts [20]. Viisainen et al attributes the variability in NCF preform results to the more 'complex architecture' [18], with NCFs consisting of intra-ply stitches rather than interlaced primary yarns. This leads to a difference in shear response, with woven fabrics shearing at the cross-over points between yarns, a mechanism that the stitches cannot emulate. In fact, studies [21] [11] have shown the asymmetry effect of stitching on a symmetric biaxial NCF draped over a symmetric shape – the hemisphere. Non-orthogonal biaxial combinations such as 0°/135° NCFs may add another level of complexity but have not been investigated in depth in the literature. This study aims to build on the knowledge of NCF forming through testing these biaxial orientations.

3. Methodology

Forming experiments were carried out on two representative aerospace geometries shown in Figure 2. The geometries contain features such as ramps, recessing web depth and corner radii. Ramps are common in aerostructures for weight and loading optimisation of the structure. The ramps selected have a gradient of 1:40 and recede towards the centre of the geometry creating an excess in fabric length. The footprint of both geometries is approximately 0.9 m x 1.9 m (chord x span length), a sizeable increase from any forming geometries currently available in the literature. Table 2 shows a full list of dimensions. The NCF material was placed on the geometry upper surface and left to drape over the vertical web and rest on the lower surface under its own weight. A non-reusable diaphragm

was sealed around the edges of each tool and vacuum was pulled until the fabric conformed to the geometry. This set up drives the kinematics of the diaphragm, starting with the top surface being pulled under vacuum followed by the male or convex radius and outside edge of the bottom surface. The last surface the diaphragm comes into contact with is the female or concave radius. The preform surface was scanned while still under vacuum with a Hexagon Absolute Arm and interrogated for wrinkle dimensions using Polyworks software.

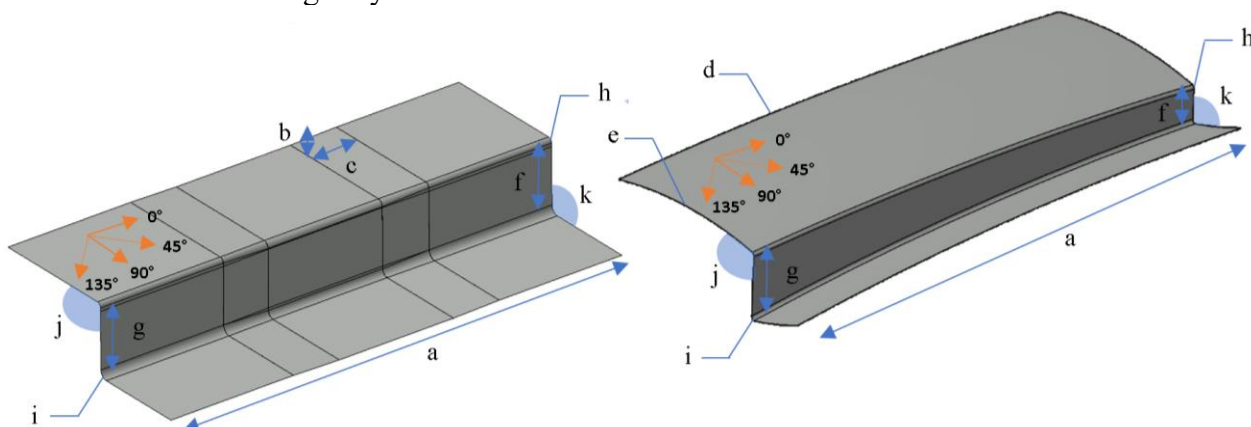


Figure 2. Representative geometries used for forming trials (labels described in Table 2).

Table 2. Representative geometries used for forming trials dimensions

Ramp geometry		Curve geometry	
Length [a] (mm)	2000	Length [a] (mm)	2000
Ramp height to length ratio [b:c]	1:40	0° to 90° radius of curvature ratio [d:e]	6
Web height ratio [f:g]	1:1	Web height ratio [f:g]	1:2
Convex to concave corner radius ratio [h:i]	1:2	Convex to concave corner radius ratio [h:i]	1:1
Top surface / web to bottom surface / web angle ratio [j:k]	1:1	Top surface / web to bottom surface / web angle ratio [j:k]	1.25:1

The preforms were assessed qualitatively through photographs and preform scans. Preform wrinkling was assessed through the use of:

- Frequency plots of wrinkle height and width data points sampled equally over the preform wrinkle area. The sampling was dependent on the scanner resolution.
- Scatter plots showing relationship between wrinkle height and wrinkle width.

Three NCF orientations were used to create the preforms. The specification of each is shown below.

Table 3. NCF specification

ID	Orientation	Stitch type	Stitch size	Binder type
NCF1	0/90	Tricot	5.1mm	Polyamide
NCF2	0/135			
NCF3	45/135			

Using combinations of these NCFs, the following matrix of trials was carried out. T4 and T8 are referred to in the text as quasi-isotropic (QI) layups.

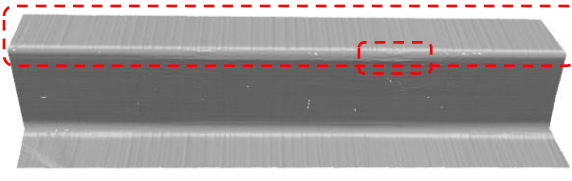
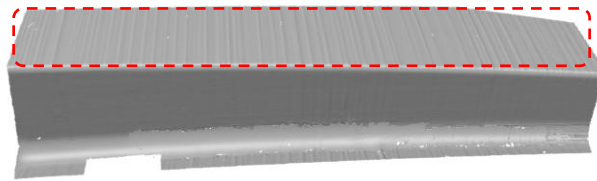
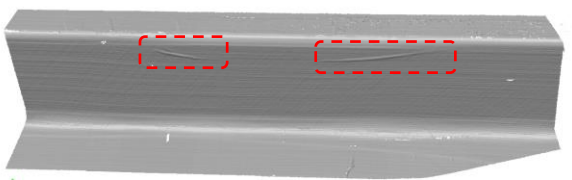
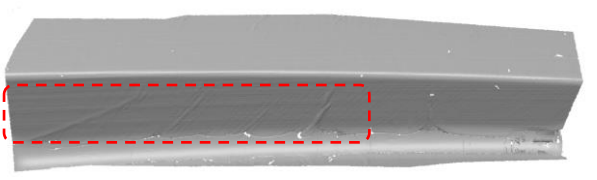
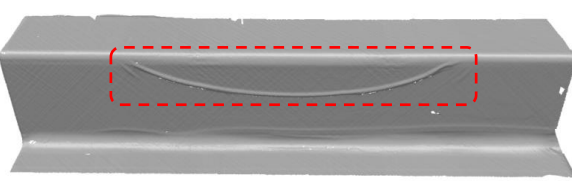
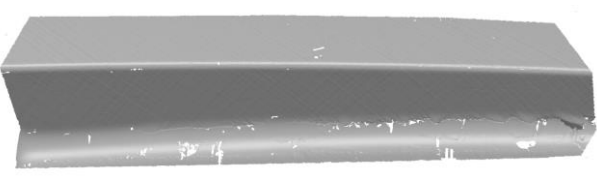
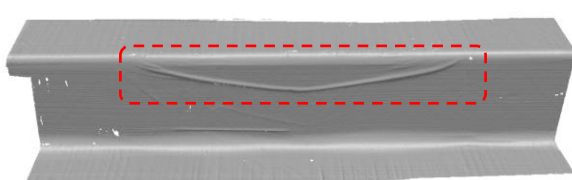
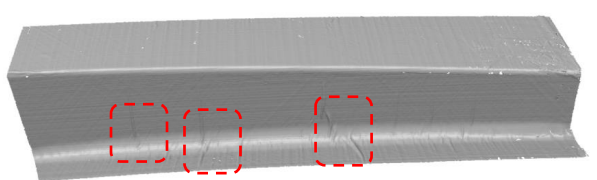
Table 4. Matrix of trials

Trial ID	NCF Ply Sequence	Geometry
T1	[0/90] ₆	Ramp
T2	[0/135] ₆	
T3	[45/135] ₆	
T4	[45/135,0/90,0/135,45/135,0/90,0/135]	
T5	[0/90] ₆	Curve
T6	[0/135] ₆	
T7	[45/135] ₆	
T8	[45/135,0/90,0/135,45/135,0/90,0/135]	

4. Results

The scanned preform results are shown in Table 5. Wrinkles have been highlighted in red. Missing data points in the scans were due to the reflection of the diaphragm and did not affect the quality of the results. The ramp geometry preforms showed a distinctive wrinkle shape on the web, initiating at the outside edges of the ramps and descending into the centre in a parabolic shape. This was most noticeable in the $45^\circ/135^\circ$ and quasi-isotropic layups, suggesting the former is the orientation driving the wrinkling in the latter. By contrast, the $45^\circ/135^\circ$ layup formed on the curve geometry showed no noticeable wrinkling. Comparing the quasi-isotropic preform on this geometry to the other three orientations, shows similarities with the non-orthogonal $0^\circ/135^\circ$ preform, with wrinkling initiating on the web of the geometry and some occurring in the concave or female radius. The orientation of the wrinkles however is different, with those on the non-orthogonal preform following the direction of the 135° fibres, whilst those in the quasi-isotropic laminate following a general vertical or 90° direction. Though the $0/90^\circ$ preforms showed no significant wrinkling on either geometry, a ‘corrugated’ effect was observed on both preforms under vacuum, whereby some fibres in the 90° direction appeared higher in amplitude (out-of-plane) than others. This phenomenon was observed in the quasi-isotropic preforms.

Table 5. Scanned preform showing wrinkle appearance

	Ramp	Curve
$[0/90]_6$		
$[0/135]_6$		
$[45/135]_6$		
QI		

The analysis of wrinkle location is complemented by photographs in Figure 3 showing close-up and overall wrinkle appearance of the different preforms. Figures 3b and 3d show the clear difference in wrinkle direction from one geometry to another – mostly in the horizontal or 0° fibre direction for the ramp geometry, and mostly vertical or 90° direction for the curve geometry. In both instances, the wrinkle crosses several NCF tows and seems unrestrained by tow size or stitch size. Though the orientation of the wrinkle relative to the geometry is different between the two, the wrinkles themselves appear similar - both showing to be out of plane of the preform and with no visible in-plane effect on fibre or tow deviation. Though the results are limited to the appearance of the outer most ply, it is assumed that the resultant wrinkle is an interaction of the six plies of biaxial NCFs in total.

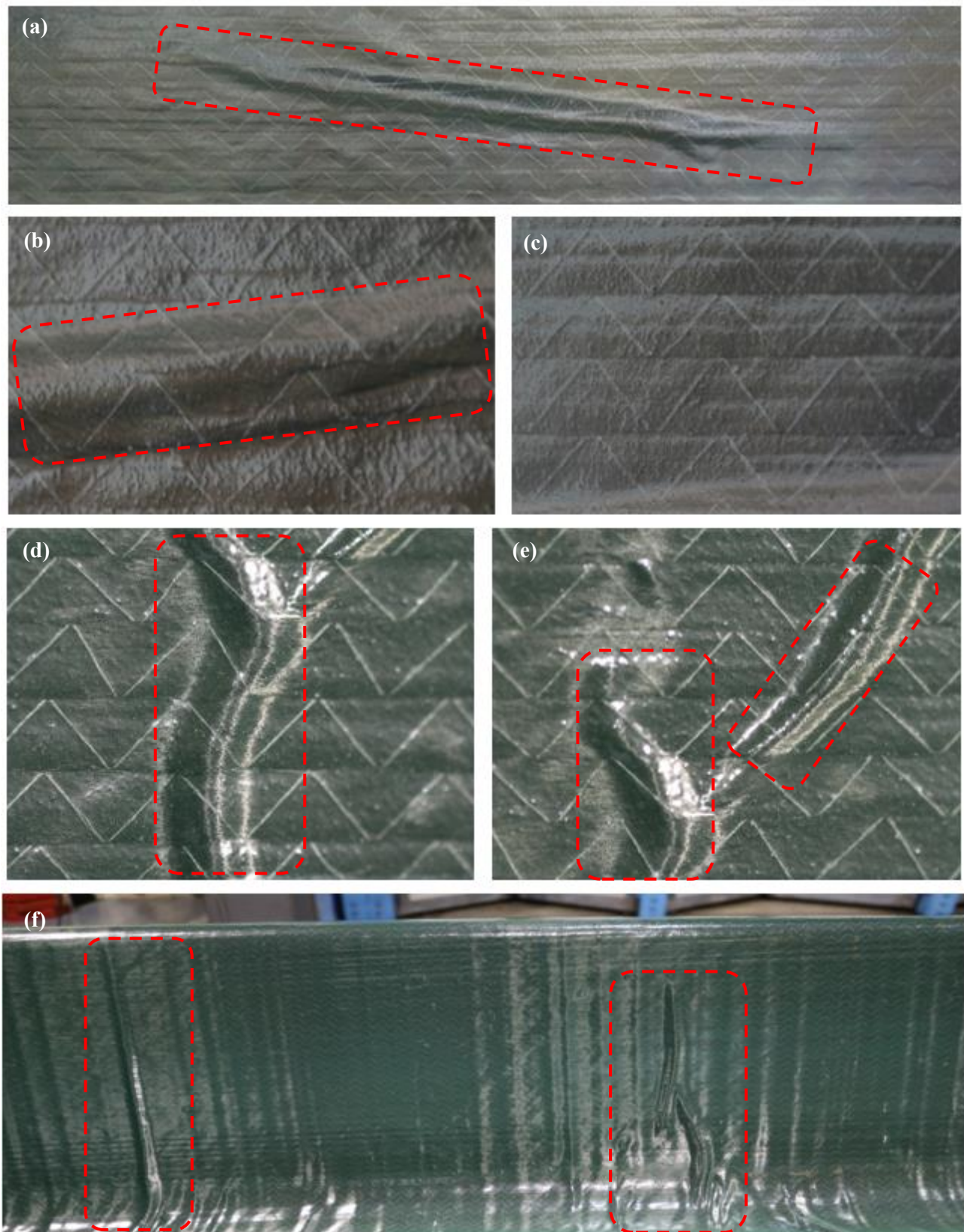


Figure 3. Appearance of wrinkles in preforms, all photographed under vacuum; (a) Wrinkle on left ramp for 0/135 layup on ramp geometry; (b) Close up wrinkle on right ramp for 0/135 layup on ramp geometry; (c) Close up of unwrinkled preform on ramp geometry for comparison; (d) & (e) Close up wrinkles on QI layup on web of curve geometry (f) Overall wrinkling on QI layup on web and bottom surface of curve geometry

Figures 4 and 5 show the frequency plot results for wrinkle heights and wrinkle widths respectively. Several wrinkle height data points are sampled in each continuous wrinkle observed in the scans in Table 5. As the sampling was dependent on the resolution of the scanner, smaller wrinkles have a smaller number of samples or data points. The frequency plots were therefore normalised to enable a

better comparison between them. No wrinkle data points are shown for the $45^\circ/135^\circ$ preform on the curve geometry (Figure 4f) as no visible out of plane wrinkles were observed. Results show the highest wrinkle heights occur in the QI preforms (Figures 4a & 4b), with the ramp geometry value skewing towards the higher values. An overall comparison of the shape of the wrinkle height distributions between the two geometries reveals a wider spread for the curve geometry than the ramp geometry, suggesting a higher variability in wrinkling behaviour. A correlation is observed between wrinkle height and wrinkle width distributions (see Figure 5 for wrinkle widths), e.g. ramp geometry values are both higher and wider than curve geometry values - suggesting these are both material driven parameters. This relationship is shown further in Figure 6.

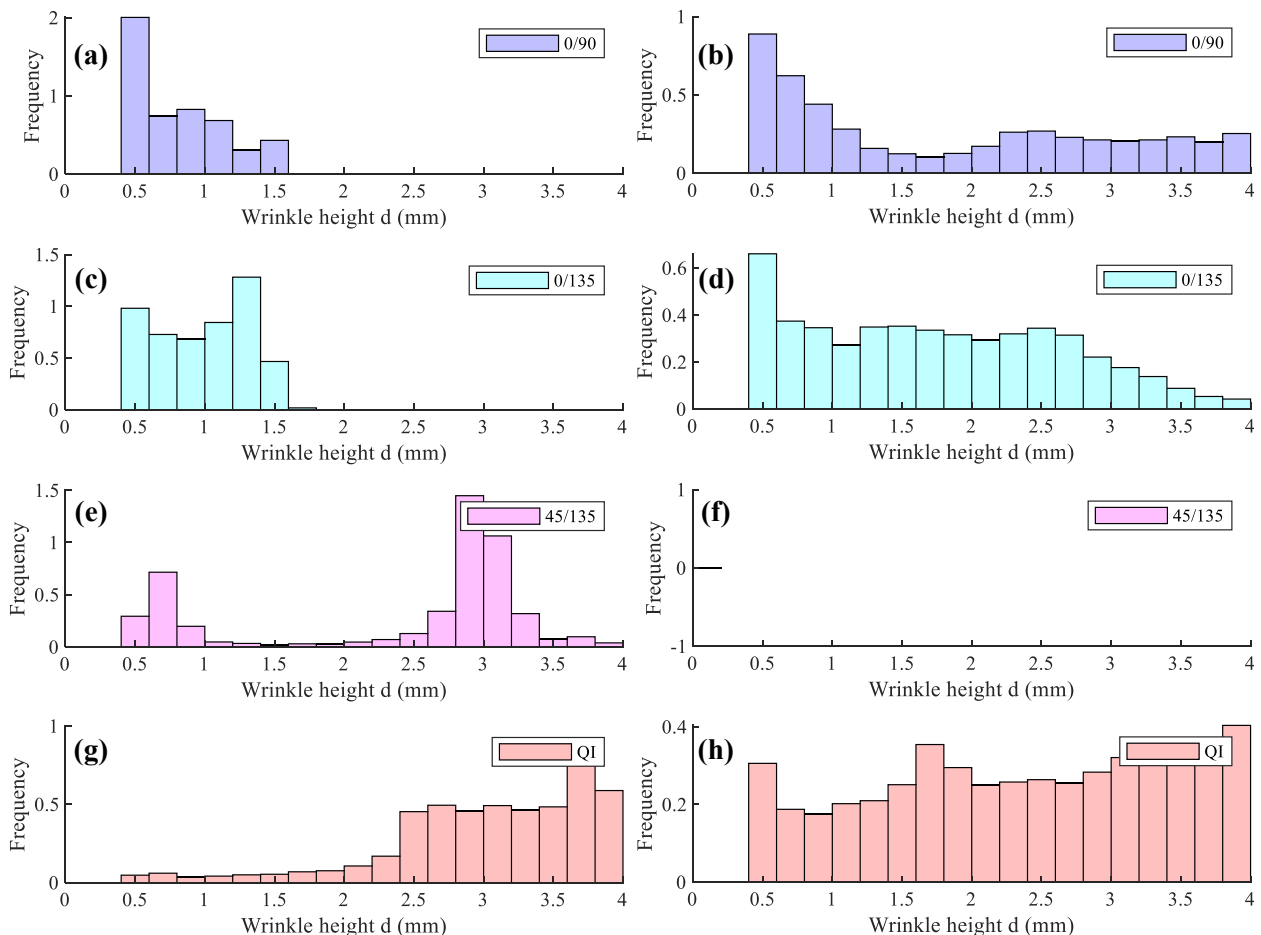


Figure 4. Frequency plots for out-of-plane wrinkle heights (several wrinkle heights sampled per wrinkle). Left: ramp geometry, right: curve geometry

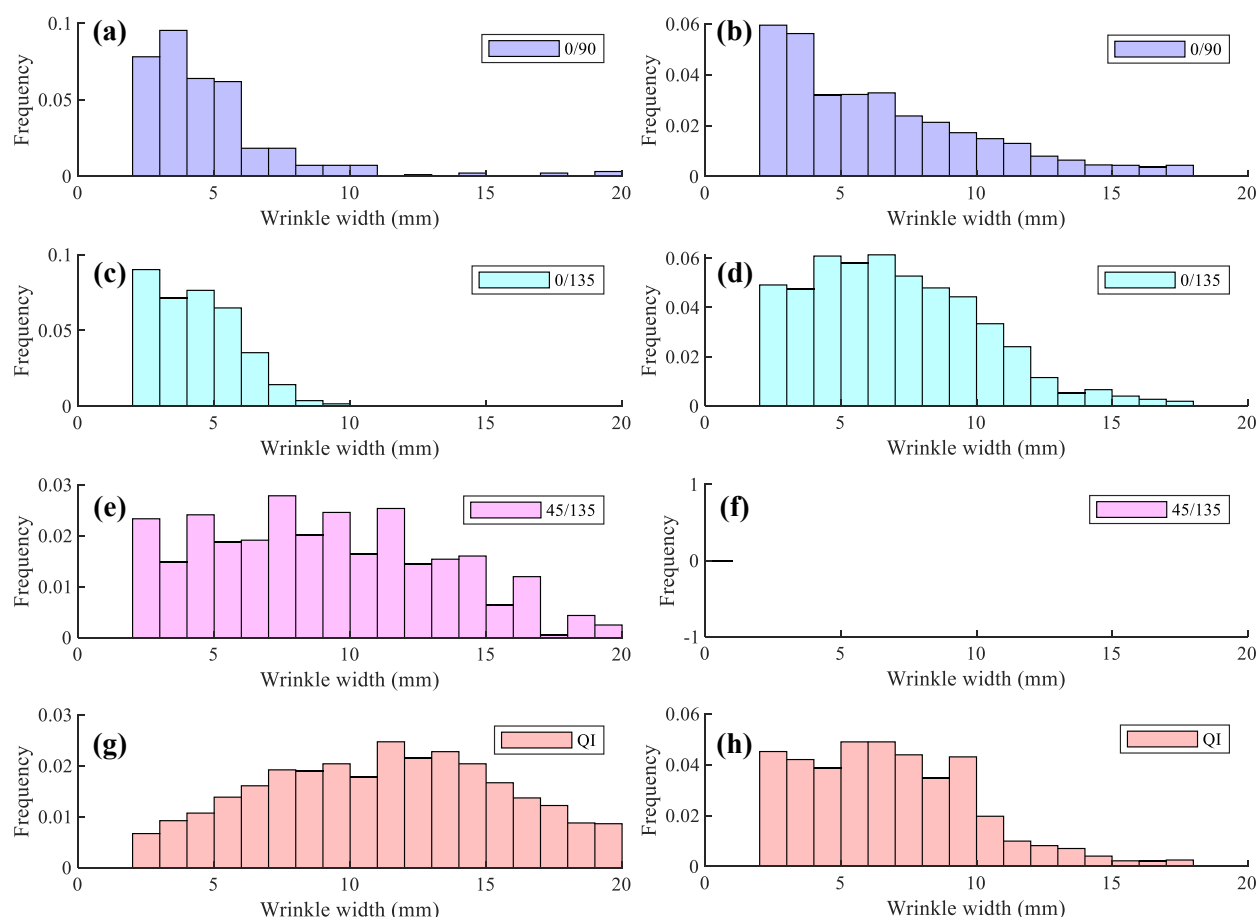


Figure 5. Frequency plots for in-plane wrinkle widths (several wrinkle widths sampled per wrinkle). Left: ramp geometry, right: curve geometry

Figure 6 shows the scatter plot and regression results for wrinkle height versus wrinkle width. Plots show the gradient of width to height (L/d) of the regression line, the coefficient for regression R^2 and the 1 ply thickness line for reference. Sampling was dependent on wrinkle area, with smaller wrinkles showing a smaller number of samples. No data points are shown for the $45^\circ/135^\circ$ preform on the curve geometry (Figure 6f) as no visible wrinkling was observed. All preforms showed a relatively high linear regression between wrinkle height and width with coefficients of 0.8 and 0.9. A comparison between these, however, should be avoided, as the sampling is not equal for all eight preforms, due to the dependence on wrinkle size. Under the same argument, a comparison can and should be made between the $45^\circ/135^\circ$ and QI preforms on the ramp geometry (Figures 6e & 6g), as these showed visibly similar wrinkle sizes and shapes. Results show a steeper height to width gradient for the single orientation over the quasi-isotropic laminate, though overall higher wrinkling is seen for the QI preform. Overall higher values in both height and width are observed for the ramp geometry than the curve geometry, suggesting a bigger amount of material excess induced through this geometry feature. However, the height to width ratio comparison between the two geometries is not conclusive, reinforcing the hypothesis that this is a material driven parameter rather than geometry driven.

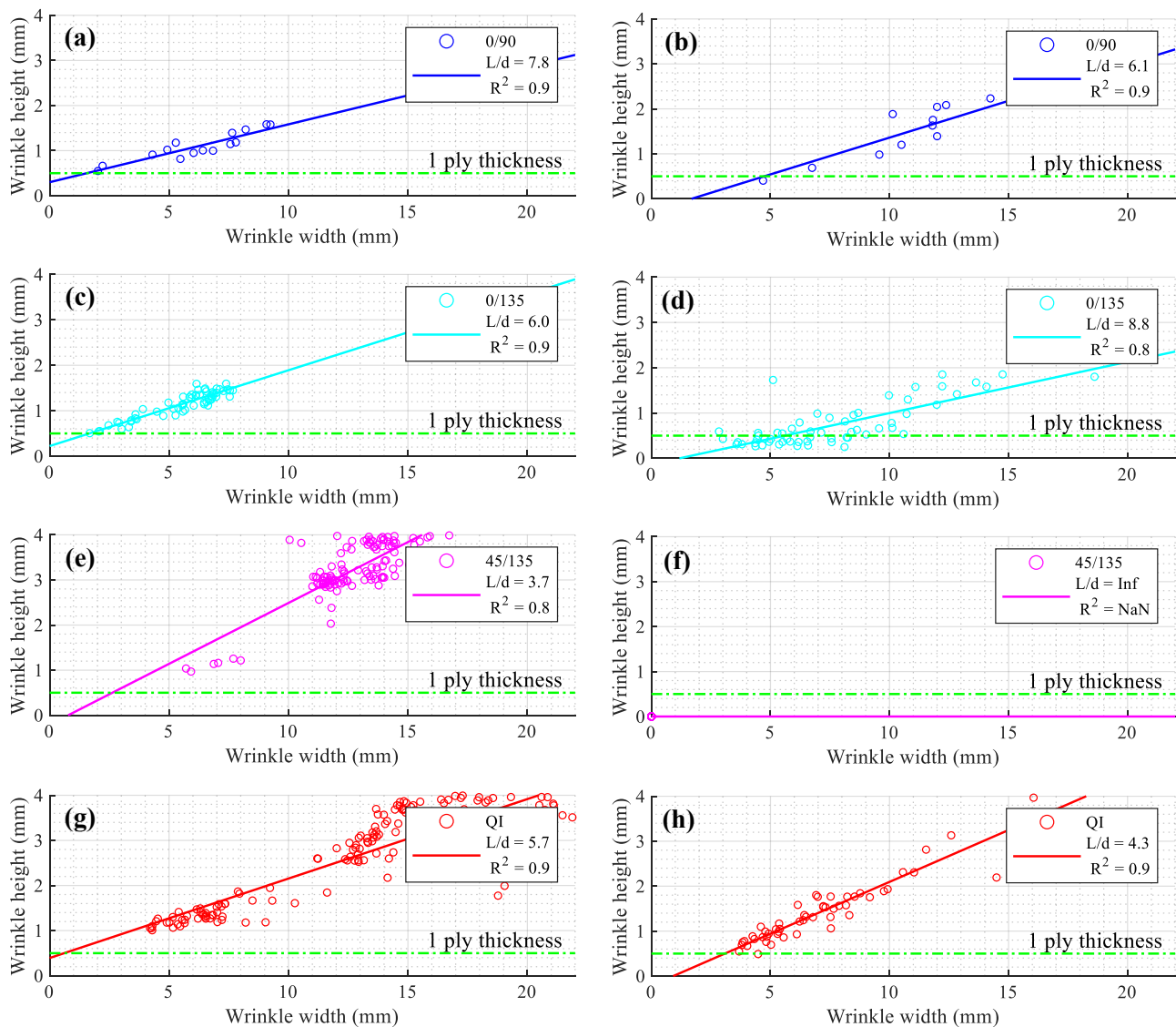


Figure 6. Scatter plots with regression lines for wrinkle height (d) vs wrinkle width values (L) (several values sampled per wrinkle). Left: ramp geometry, right: curve geometry

5. Discussion

This study has focused on two large scale representative geometries appropriate for subcomponent testing. One geometry is analogous to Hallander's spar geometry [22] with two transition zones (or ramps) leading to a recess area in the centre in both surfaces and web, while the other shows double curvature on the surfaces joined by a straight web. Instead of two convex radii, the geometries have the added complexity of a convex to concave radius transition, which can lead to issues such as over-consolidation and bridging respectively, as shown by Chen et. al. [23]. In fact, bridging was visibly noticeable on the curve geometry, most likely caused by the acute angle between the centre web and bottom surface by comparison to the ramp geometry. While the radii of curvature seen on the top surface of the curve geometry are not as aggressive as those available in the literature in the form of hemispherical punch set ups, the added complexity of a convex radius (of much tighter dimensions than those of curvature) transitioning into a flat planar surface is a forming challenge. This was observed in the results in the form of out-of-plane wrinkling on the web and bottom surface. The location of the wrinkling is due to a combination of the drape sequence and the geometric complexities. Figure 7 shows the drape sequence of the diaphragm on either end (left and right) of each geometry, numbered from 1 (diaphragm touches down on geometry first) to 4 (diaphragm touches down on geometry last). For both geometries, the top surface is 'clamped' under vacuum first, followed by the top convex radius and the outside edge of the bottom surface. This is due to

how the diaphragm is secured on to the tooling geometries. The last surface under vacuum is the concave lower radius, leading to potential problems in bridging. Whereas the ramp geometry shows a 'symmetric' drape sequence (about the plane of symmetry drawn in Figure 7), the recessing web depth of the curve geometry leads to a slight delay in the drape sequence of the left side (deep web depth) over the right side (shallow web depth). This leads to material excess gathering towards the deeper web area.

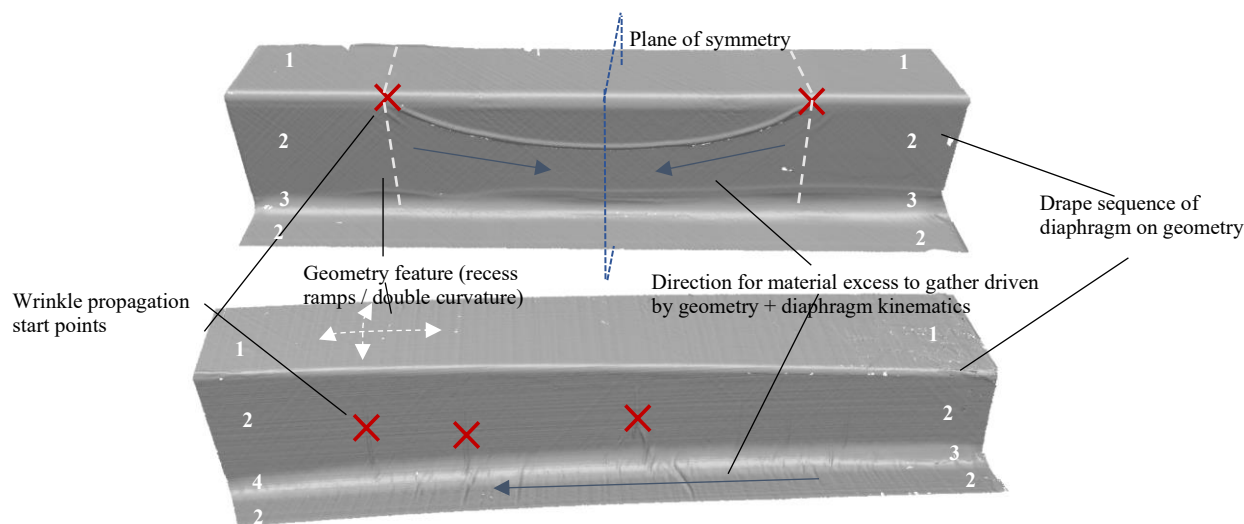


Figure 7. Diagram of drape sequence in relation to resultant preform wrinkling for ramp geometry (above) and curve geometry (below)

The effect of symmetry can be seen in the resulting wrinkle shapes, with the ramp geometry showing an almost repeatable symmetric central wrinkle for all laminates with 45° fibres in them. Curiously, the non-orthogonal and asymmetric $0^\circ/135^\circ$ preform showed the least symmetry in terms of wrinkle shape, suggesting if both geometry and laminate share a symmetry plane, the resultant defect may also be symmetric. This hypothesis holds true for the asymmetric behaviour observed in Chen et. al.'s [23] work over a hemisphere, as a hemisphere has an infinite number of planes of symmetry (perpendicular to its flat bottom surface), whereas an orthogonal $45^\circ/135^\circ$ stitched NCF laminate only has two (in the direction of the stitch, and perpendicular to the stitch, both through the centre point of the laminate).

Though it is widely known that both geometry and material are two influencing parameters in the forming, this study has helped isolate these two parameters and contrast them against each other. Perhaps the most noticeable result was the seemingly 'perfect' (no wrinkling) $45^\circ/135^\circ$ preform on the curve geometry by contrast to the ramp geometry – showing an example of a 'pure' geometry-driven forming. The 45° fibres' path length over the ramp buckle over each other as there can be no sliding between them unlike for the 90° fibres over the same geometry. This is due to the 90° fibres' orientation relative to the ramp, whereas these form over the feature, the sliding between them is able to accommodate the change in path length. The same hypothesis can be applied to the 0° fibres on the curve geometry, where the change in path length due to the combination of the curved upper surface and convex radius leads to buckling of the fibres. The $0^\circ/135^\circ$ preform on the curve geometry shows that this buckle in the 0° fibres propagates along the second stitched fibre direction, in this case along the 135° . With the addition of 90° in the quasi-isotropic laminate, the orientation of the wrinkles approximates these showing the interaction between these two orientations. However, the nature of the wrinkling observed in the curve geometry – sporadic and spread out, suggests a higher variability should repeats of the trials be performed. By contrast, the ramp geometry's relatively repeatable wrinkle shape places the geometry as a potential baseline for an industrial material characterisation test campaign.

Variability was also observed in the wrinkle height and width frequency plot results, where the curve geometry showed an overall higher spread in distribution than the ramp geometry. The aspect ratio (wrinkle width versus height) results reinforced this as a material parameter, driven by the bending

stiffness of the fabric rather than dependent on geometry. Similarities in aspect ratio and values were observed between the preforms that were visibly most similar, e.g. the 45°/135° and QI laminate for the ramp geometry. The same similarities were not as clear for the curve geometry, reinforcing the argument for higher variability and lower repeatability shown for this geometry. Lower wrinkle heights were observed for smaller area wrinkles suggesting an aspect ratio ‘ramp up’ along the length of a fully developed wrinkle must occur. This is supported by an overall high level of regression between wrinkle width and height.

6. Concluding Remarks

This study follows the footsteps of many drapability studies published already, as highlighted in the literature review, but introducing results on industrial scale geometries. This means the size and types of defects observed in the preforms are representative of those in a full scale aerostructures. The choice of geometries pose a challenge to NCF forming with features like recess ramps, double curvature and radii corners. The differences observed in wrinkle size, type and orientation between the two geometries show the importance of this parameter to the final preform result. The results from the three bi-axial NCF formats suggest the existence of a ‘driving’ format or orientation when measured via resulting preform wrinkles and reinforces the effect of geometry as a key parameter for drapability of NCFs. Though the industrial value of draping at this scale is clear, the resource and time intensive nature of the trials does place them at a disadvantage to benchtop geometries explored in the literature review. While the building block approach to industrial test pyramids remains, the geometries presented show potential as benchmarking tools to characterise defects likely to be seen on a full size aerostructure.

7. Acknowledgements

This work was supported by the EPSRC Centre for Doctoral Training in Composites Manufacture (EP/L015102/1) and the Airbus Wing of Tomorrow programme, part funded by the UK’s Aerospace Technology Institute. The authors would like to thank the National Composites Centre in Bristol for test data collection, and Airbus colleagues Jon Wright, Jon Price, and Dominic Bloom for many interesting discussions on composite forming.

References

- [1] M. A. Turk, B. Vermes, A. J. Thompson, J. P. H. Belnoue, S. R. Hallett, and D. S. Ivanov, “Mitigating forming defects by local modification of dry preforms,” *Compos. Part A Appl. Sci. Manuf.*, no. October, p. 105643, 2019.
- [2] S. Lomov, *Non-Crimp Fabric Composites: Manufacturing, Properties and Applications*. Woodhead Publishing Series in Composites Science and Engineering, 2016.
- [3] A. J. Thompson, B. El Said, J. P. Belnoue, and S. R. Hallett, “Modelling process induced deformations in 0 / 90 non-crimp fabrics at the,” *Compos. Sci. Technol.*, vol. 168, no. January, pp. 104–110, 2018.
- [4] D. Adams, “Composites testing as part of a building block approach, Part 2: Upper building block levels,” *Composites World*, Nov-2021.
- [5] S. Allaoui, C. Cellard, and G. Hivet, “Effect of inter-ply sliding on the quality of multilayer interlock dry fabric preforms,” *Compos. Part A Appl. Sci. Manuf.*, vol. 68, pp. 336–345, 2015.
- [6] F. Nosrat Nezami, T. Gereke, and C. Cherif, “Active forming manipulation of composite reinforcements for the suppression of forming defects,” *Compos. Part A Appl. Sci. Manuf.*, vol. 99, pp. 94–101, 2017.
- [7] E. Capelle, P. Ouagne, D. Soulat, and D. Duriatti, “Composites : Part B Complex shape forming of flax woven fabrics : Design of specific blank-holder shapes to prevent defects,” *Compos. PART B*, vol. 62, pp. 29–36, 2014.

-
- [8] P. Hallander, M. Åkermo, C. Mattei, M. Petersson, and T. Nyman, "Composites : Part A An experimental study of mechanisms behind wrinkle development during forming of composite laminates," *Compos. Part A*, vol. 50, pp. 54–64, 2013.
- [9] Airbus, "A320neo: The most successful commercial aircraft family ever." [Online]. Available: <https://aircraft.airbus.com/en/aircraft/a320/a320neo>.
- [10] D. I. N. Spec, A. Pr, and T. Deutsch, "DRAPETEST Patent," no. November, 2015.
- [11] G. Bardl *et al.*, "Analysis of the 3D draping behavior of carbon fiber non-crimp fabrics with eddy current technique," *Compos. Part B Eng.*, vol. 132, pp. 49–60, 2018.
- [12] F. Nosrat, T. Gereke, and C. Cherif, "Composites : Part A Analyses of interaction mechanisms during forming of multilayer carbon woven fabrics for composite applications," *Compos. PART A*, vol. 84, pp. 406–416, 2016.
- [13] P. Hallander, J. Sjölander, M. Petersson, and M. Åkermo, "Interface manipulation towards wrinkle-free forming of stacked UD prepreg layers," *Compos. Part A Appl. Sci. Manuf.*, vol. 90, pp. 340–348, 2016.
- [14] P. Hallander, J. Sjölander, and M. Åkermo, "Forming induced wrinkling of composite laminates with mixed ply material properties; an experimental study," *Compos. Part A Appl. Sci. Manuf.*, vol. 78, pp. 234–245, 2015.
- [15] P. Harrison, R. Gomes, and N. Curado-correia, "Composites : Part A Press forming a 0 / 90 cross-ply advanced thermoplastic composite using the double-dome benchmark geometry," *Compos. Part A*, vol. 54, pp. 56–69, 2013.
- [16] M. A. Khan, T. Mabrouki, and P. Boisse, "Journal of Materials Processing Technology Numerical and experimental analyses of woven composite reinforcement forming using a hypoelastic behaviour . Application to the double dome benchmark," vol. 210, pp. 378–388, 2010.
- [17] M. A. Turk, B. Vermes, A. J. Thompson, J. P.-H. Belnoue, S. R. Hallett, and D. S. Ivanov, "Mitigating forming defects by local modification of dry preforms," *Compos. Part A Appl. Sci. Manuf.*, no. October, p. 105643, 2019.
- [18] J. V Viisainen and M. P. F. Sutcliffe, "Characterising the variability in wrinkling during the preforming of non-crimp fabrics," *Compos. Part A*, vol. 149, no. April, p. 106536, 2021.
- [19] E. Guzman-Maldonado, P. Wang, N. Hamila, and P. Boisse, "Experimental and numerical analysis of wrinkling during forming of multi-layered textile composites," *Compos. Struct.*, vol. 208, no. April 2018, pp. 213–223, 2019.
- [20] K. Tanaka, R. Ushiyama, T. Katayama, S. Enoki, and H. Sakamoto, "Formability evaluation of carbon fiber NCF by a non-contact 3D strain measurement system and the effects of blank folder force on its formability," *WIT Trans. Built Environ.*, vol. 137, pp. 317–326, 2014.
- [21] S. Chen, O. P. L. McGregor, L. T. Harper, A. Endruweit, and N. A. Warrior, "Composites : Part A Defect formation during preforming of a bi-axial non-crimp fabric with a pillar stitch pattern," *Compos. Part A*, vol. 91, pp. 156–167, 2016.
- [22] P. Hallander, M. Åkermo, C. Mattei, M. Petersson, and T. Nyman, "An experimental study of mechanisms behind wrinkle development during forming of composite laminates," *Compos. Part A Appl. Sci. Manuf.*, vol. 50, pp. 54–64, 2013.
- [23] S. Chen *et al.*, "Double diaphragm forming simulation for complex composite structures," *Compos. Part A Appl. Sci. Manuf.*, vol. 95, pp. 346–358, 2017.